Electron Beam Visualization in Hypersonic Airflows

H. F. Lee*
Air Force Flight Dynamics Laboratory Wright-Patterson Air Force Base, Ohio
and
S. L. Petrie†
Ohio State University, Columbus, Ohio

The electron beam fluorescence technique has been employed for visualizing hypersonic airflow fields. A high current electron beam generator was used to provide electron beams with currents up to 50 ma at voltages up to 20 kv. Applications of the technique at low densities illustrate that many details of the flowfield can be obtained in density regions where conventional optical systems fail to yield useful results. Techniques for obtaining quantitative density measurements with photographic techniques are discussed. The value and versatility of the method is demonstrated by results obtained with a sharp cone model and an advanced ramjet aircraft configuration in a Mach 10 airflow field.

Introduction

IT is well-known that conventional optical methods of flow visualization fail under low density conditions typical of hypersonic wind tunnel facilities. In particular, interferometer and schlieren techniques frequently yield only the structure of very strong shock waves in such flowfields and additional details concerning boundary layer and wake structure cannot be examined.

Because of the failure of these methods in many hypersonic test facilities, various low density flow visualization techniques have been developed and are summarized in Ref. 1. These include excitation of gas molecules by electron impact produced by high-voltage d.c. or a.c. glow discharges, x-ray and ultraviolet absorption techniques, and the electron optical schlieren method. These techniques may provide rough quantitative density distributions within the flowfield and/or provide correct density measurement but require elaborate and expensive set-ups. Frequently, they give flow images which are of poor contrast.

The electron beam fluorescence technique has received considerable attention for the measurement and visualization of low density flows where conventional optical techniques become insensitive. In this technique, a narrow beam of electrons is projected across the flowfield and the interaction of the electrons with gas particles produces a column of radiation nearly coincident with the beam. In certain ranges of gas density, the intensity of the electron beam-induced fluorescence varies linearly with gas density. Hence, if a photograph of the flow is taken, both qualitative and quantitative measurements can be obtained. A calibration of the sensitivity of the film can be used with standard film data reduction techniques to yield actual density distributions.

The electron beam can be traversed mechanically through the flowfield or it can be swept through a prescribed total angle electromagnetically. High beam voltages are normally used to reduce elastic scattering of the electrons so that a thin beam is produced. By proper adjustment of the sweeping voltages, either the entire flowfield can be illuminated or an arbitrary "two-dimensional" slice out of the flowfield can be examined. This latter feature made the electron beam particularly attractive for the examination of flows about complex aerodynamic shapes.

When the electron beam is mechanically traversed through the flowfield,[1] time-exposure photographs can be obtained to yield visualization in arbitrary gas mixtures. In this case, however, the wind tunnel run time is long and only steady-state flow phenomenon can be investigated.

Application of afterglow techniques requires the presence of long-lived excited particles in the flowfield downstream of the electron beam; the afterglow method has been particularly successful in nitrogen[2,3] and helium[4,5] flowfields. However, attempts to employ either the afterglow radiation or electromagnetic sweeping of the beam in hypersonic airflows has generally been unsuccessful. It is notable that visualization in airflows depends upon excitation of molecular nitrogen by high-speed electrons and it is well-known that nitrogen-oxygen collisions result in earlier quenching of radiation as the density is increased than do either nitrogen-nitrogen or in nitrogen-helium collisions.[6] In addition, no after-glow radiation outside the main area of excitation is observed in airflows while such observations are common in nitrogen and helium. The afterglow radiation is reponsible, in part, for the successful application of a swept electron beam in nitrogen and helium. The absence of the afterglow radiation in airflows may be responsible for past failures of the method.

In usual applications of the electron beam for flow visualization, electron beams with voltages from 10 to 100 kv and beam currents of a few milliamperes are employed. It is expected that application of image intensifier techniques[7] to airflows will yield useful visualization data. However, this requires complicated photographic equipment. Another approach to obtain useful data is to employ an electron beam with a current high enough to yield sufficient photographic exposure in the absence of afterglow radiation. The results of such an application are reported here.

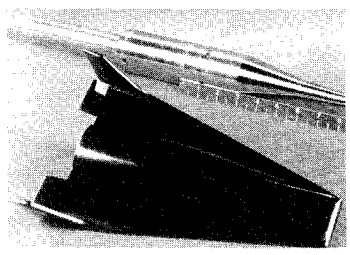

Fig. 1 Top view of ramjet fighter model.

Presented as Paper 72-1017 at the AIAA 7th Aerodynamic Testing Conference, Palo Alto, Calif., September 13-15, 1972; submitted October 2, 1972; revision received February 1, 1973. This research was sponsored under Contract F33615-72-C-1023, Air Force Flight Dynamics Laboratory, Wright-Patterson Air Force Base, Ohio. The authors wish to thank R. F. Carpenter, D. M. Parobek, G. W. Williams, and R. L. Lickert, Air Force Flight Dynamics Laboratory, for their advice and contributions.

Index categories: Supersonic and Hypersonic Flow; Research Facilities and Instrumentation.

*Project Engineer.

†Professor, Department of Aeronautical and Astronautical Engineering. Member AIAA.

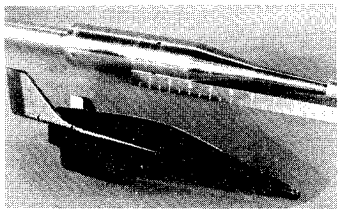

Fig. 2 Side view of ramjet fighter model.

A high current electron beam was used to provide visualization of low density airflow fields. Particular emphasis was placed on flow regimes where conventional schlieren techniques yield little or no useful data. Combined schlieren and electron beam data were obtained at certain wind tunnel operating conditions to allow comparisons of the sensitivities of the two systems.

Apparatus and Procedure

Wind Tunnel and Model Systems

The flow visualization studies were conducted in the High Temperature Facility (HTF) operated by the Flight Mechanics Div. of the Air Force Flight Dynamics Lab. (AFFDL). The facility consists of a pebble-bed heater, a contoured convergent-divergent nozzle, a freejet test cabin, and a pressure recovery system. For the studies reported here, the tunnel was operated with air at a reservoir temperature of 2500°R with reservoir pressures varying from 100 to 600 psia. The nominal nozzle exit Mach number was 10.

To establish the feasibility of obtaining quantitative data from the flow visualization technique, a series of wind tunnel tests was conducted with a sharp 9° half-angle cone at various angles of attack. The cone was fitted with an annular injection port at its base so that massive base blowing could be simulated. Both air and helium were used for the plume gas.

Visualization of the flow about an advanced ramjet aircraft configuration was obtained to illustrate application of the technique to complicated aerodynamic shapes. This model was mounted on a pitch-roll mechanism such that arbitrary combinations of angles of attack and roll could be obtained. The model is shown in Figs. 1 and 2.

Duoplasmatron-Electron Beam System

The duoplasmatron-electron beam generator is shown schematically in Fig. 3 and is described in detail in Ref. 8. It consists of a duoplasmatron-electron source, einzel lens optics for beam forming, and electromagnetic beam steering and focusing systems. The einzel lens is mounted inside a 6 in. standard steel tee which is connected to a 6 in. oil diffusion pump. A baffle is used between the diffusion pump and the beam chamber to reduce backstreaming of the diffusion pump oil. The electrons exit from the beam chamber through a 0.03 in. diam exit orifice. The entire assembly is mounted inside the wind tunnel test cabin such that the electron beam is projected downward through the nozzle centerline. The electron beam power supplies and vacuum control console are located in a control panel adjacent to the tunnel. The beam generator is electrically isolated from the test cabin so that no special beam collecting devices are required; that is, the tunnel test cabin serves as a beam receiver.

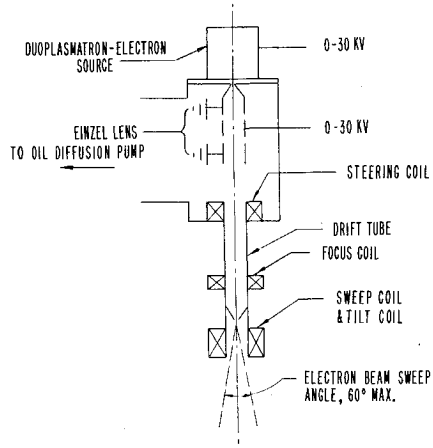

Fig. 3 Duoplasmatron-electron beam generator schematic.

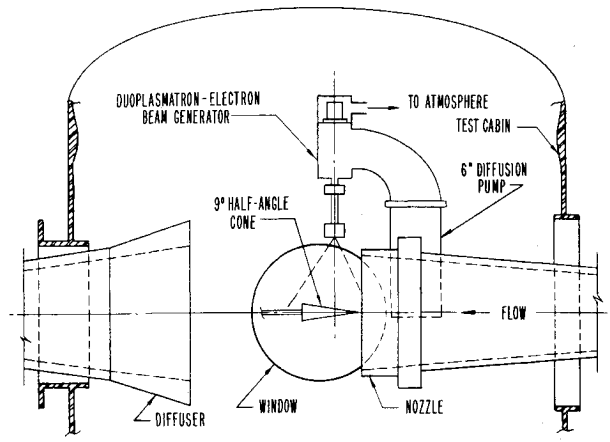

Fig. 4 Electron beam installation in AFFDL/HTF.

The maximum acceleration potential is 20,000 v with a maximum beam current of 50 ma. To minimize defocusing of the beam as it traverses the drift tube and passes through the exit orifice, the electrons are accelerated from high potentials toward ground potential. Hence, the duoplasmatron power supplies must be operated at high potential and electrical isolation from ground must be maintained.

Electromagnetic sweeping of the beam is accomplished with a sweep coil located immediately beneath the exit orifice. A triangular current wave form in the deflection coil generally is best suited for flow visualization work, since the electron beam moves at a constant rate and will yield a constant exposure with deflection angle on the film. In addition, a high sweep frequency is desirable to provide many passes of the electron beam during the photographic exposure time. (For example, a 60 cycle sweep frequency will yield some "flicker" in movies taken at 24 frames per second.)

In addition to sweeping the beam, the tilt coil can be used to locate the electron beam in any desired position within the test gas. A d.c. bias system is supplied to provide an offset current through both sets of coils making up the deflection yoke. The sweeping voltage is capacitance-coupled to one set of coils. Adjustment of the plane of the sweep is accomplished simply by rotating the deflection yoke on the drift tube.

The duoplasmatron-electron beam generator installation in the HTF is shown schematically in Fig. 4. The test configuration with the ramjet fighter aircraft model is shown in Fig. 5. The exit of the tilt coil is just visible at the upper edge of this photograph.

Double Pass Schlieren System

The double pass schlieren system consists of a parabolic mirror, a plane mirror (each has an adjustable stand) and the remaining optics mounted on an optical bench. All optics on the bench are located on the centerline of the parabolic mirror. The test region and the plane mirror are in the upper half of the parallel beam from the large parabolic mirror.

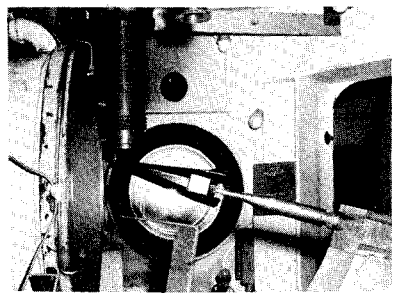

Fig. 5 Electron beam and test model in AFFDL/HTF.

The light source is an Osram HBO 200 w short arc mercury lamp. The light from the lamp is focused on a 1/2 mm square aperture which serves as the entrance slit for the schlieren system. This slit is located at the focus of the parabolic mirror. The parallel light reflected from the parabolic mirror passes through the test cabin and is reflected back through the cabin again, to the parabolic mirror through a beam splitter and a magnifying lens to a horizontal knife edge, another beam splitter, and a camera lens to a 35 mm camera body as shown in Fig. 6.

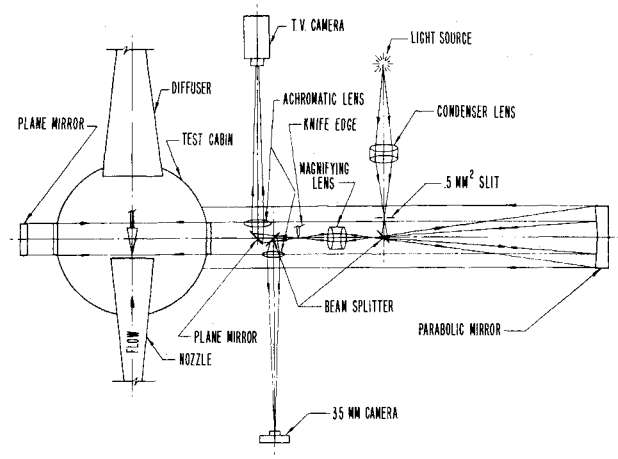

Fig. 6 AFFDL/HTF 20 in. diam double pass schlieren system.

Experiments and Discussion

General Considerations

To establish the density ranges where both quantitative and qualitative density measurements are possible, the overall excitation-emission process resulting in the observed radiation must be examined in detail. This is obviously important for quantitative density determinations but is also required for flow visualization since the manner in which the intensity of the fluorescence varies with density must be known to properly interpret flow visualization photographs. Conventional optical techniques respond to the density, the density gradient or the derivative of density gradient regardless of the density level. However, the response of electron beam induced intensity depends upon the density range investigated.

Of the many processes which can occur with excitation, excitation by secondary electrons, and collision quenching will be considered here. For excitation of molecular nitrogen these are the only mechanisms of importance. The overall intensity of radiation induced by electron excitation can be given by[8]

$$I = \frac{c\rho J Q_0 X_i}{1 + \Sigma_i(\rho_i/\rho_i')} + \frac{c\rho^2 J Q_s X_i}{1 + \Sigma_i(\rho_i/\rho_i')} \times \frac{\Sigma_i Q_{i_T} X_i/\rho \Sigma_i Q_{i_s} + \lambda_s^2}{} \quad (1)$$

where ρ is the gas density, J is the beam current, Q_0 is the cross section for excitation by primary electrons, Q_s is the cross section for excitation by secondary electrons, ρ_i' is a quenching density of species i, Q_{i_s} is the cross section for excitation of species i by secondary electrons, Q_{i_T} denotes the total ionization cross section for species i, X_i is the number density fraction of species i, λ_s is related to the mean free path for secondary electrons, and c is a constant depending on geometrical factors.

The radiation intensity due to excitation by primary electrons is contained in the first term of Eq. (1) while the radiation intensity resulting from excitation by secondary electrons is given by the second term. The influence of collision quenching is contained in the term $1 + (\rho/\rho')$. If the influence of secondary electrons can be neglected, Eq. (1) can be given by

$$I_0/I = 1 + (\rho/\rho') \quad (2)$$

where I_0 is the intensity in the absence of quenching. The quenching density ρ' is the density at which the intensity is reduced to 1/2 the value obtained with no quenching.

When the radiation is due almost entirely to excitation by secondary electrons, the first term of Eq. (1) can be neglected giving an intensity (in the absence of collision quenching) as

$$I = cJ\rho Q_T(\rho/\rho + k) \quad (3)$$

In this equation, the term $\rho/(\rho + k)$ is the fraction of the total radiation observed where $k = \lambda_s^2/Q_s$. At very low gas densities, the range of the secondary electrons is large such that $k \gg \rho$. In this case the radiation intensity is proportional to ρ^2. At higher densities, the range of the secondary electrons is reduced such that $\rho \gg k$ and the intensity varies linearly with density.

At gas densities less than those corresponding to 0.5 torr at room temperature, the radiation in air is dominated by the N_2^+ first negative system in the wavelength region near 4,000Å. In this case, excitation by primary electrons dominates and the second term of Eq. (1) can be neglected. Since the self-quenching equivalent pressure‡ for the N_2^+ first negative system is approximately 1.2 torr (Ref. 9), in this density region the intensity varies linearly with gas density. At equivalent pressures much over 3 torr, the N_2^+ first negative system is quenched and the N_2 second positive system becomes most intense.

The excitation cross section for the N_2 second positive system is approximately two orders of magnitude greater for secondary electrons than it is for primary electrons. Hence, the radiation in this system is due almost entirely to excitation by secondary electrons and the radiation intensity is described by Eq. (3). At very low gas densities, the intensity of the second positive system thus varies with the square of the density while at higher densities, the intensity varies linearly with the density.

The appearance of several radiation systems accompanying electron excitation obviously complicates flow visualization and quantitative determination of gas density with photographic techniques. At low gas pressures, the

‡Equivalent pressure is defined as the pressure corresponding to the actual density and a temperature of 300°K.

Fig. 7 Electron beam view of exhaust plume interaction with conical flowfield.

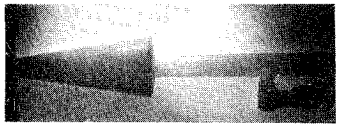

Fig. 8 Electron beam view showing wave in cone flow wake.

N_2^+ first negative system is most useful since its radiation intensity varies linearly with density. At equivalent pressures over approximately 3 torr, the N_2 second positive system is most useful. However, in intermediate regimes, both radiation systems will contribute to the total intensity and the variation of the intensity with gas pressure will be nonlinear. Radiation from these two systems can be separated with narrow bandpass interference filters set to pass radiation corresponding to a given vibrational-rotational band in the desired emission system. However, this is accomplished only at the expense of overall intensity.

Comparisons of Electron Beam and Schlieren Flow Visualization

To establish the required exposure times for the various photographic equipment employed during the wind tunnel tests, a series of static experiments was conducted. The HTF test cabin was evacuated to maintain the static pressure ranging from 1 torr up to 5 torr, and the duoplasmatron-electron beam was operated in the sweeping mode to determine the appropriate exposure times of Polaroid B&W Type 52 (ASA 400) and Polaroid Polarcolor Type 58 (ASA 75) films. These pressure conditions bracketed the expected gas densities in the body flowfields. After a series of static calibrations, the feasibility of obtaining flow patterns by the photographic method was firmly established.

The electron-induced radiation was photographed with a variety of films using 4 in. by 5 in. and 35 mm cameras as well as 16 and 35 mm movie cameras. Details of the films, the model and the tunnel operating conditions are summarized in Table I. Photographs also were obtained with the double pass schlieren system under the same test conditions as those employed with the electron beam.

Cone Flow

Electron beam and schlieren photographs of the cone flowfield were obtained with various amount of base-blowing. At the 100 psia operating condition, schlieren failed to show the bow shock wave while the electron beam yielded visualization of the entire flowfield. At the 300 psia pressure, only the bow shock was observable in the schlieren photographs, while the electron beam gave shock layer and wake details. When helium is used for the base blowing, color photography can be used to examine the extent of helium diffusion throughout the flowfield. The electron-induced radiation in helium is most intense in the region near 5,400 Å while that in air is most intense near 4,000 Å.

In Fig. 7 the separation on the cone surface caused by the interaction of the plume with the cone shock layer is clearly observable. The photograph of Fig. 8 shows a shock wave present in the cone wake. The wave is caused by downstream pressure influences and its unsteady behavior was studied with 35 mm movies. The photograph of Fig. 8 is a reproduction of one frame of these movies.

Another feature of the electron beam diagnostic technique is evident in Figs. 7 and 8. The presence of the model with base blowing causes sufficient blockage of the tunnel to raise the test cabin pressure which forces an oblique shock to form at the nozzle exit. In low Reynolds number studies when the quality of the flow is questioned, it must be examined with pitot probes, since conventional schlieren systems will not operate at these densities. Probing of the flow with a pitot probe is a perturbing and time consuming process as well as having a limited response to dynamic effects. However, the formation of the nozzle exit shock wave can clearly be seen in the electron beam photographs of Figs. 7 and 8.

For all of the electron beam photographs, the beam was operated in the sweeping mode. Preliminary experiments were conducted to determine if there was any afterglow radiation sufficient for photographic purposes. No afterglow was observed and the radiation was restricted to the region excited by the primary electrons.

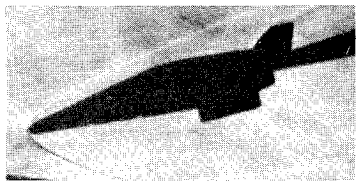

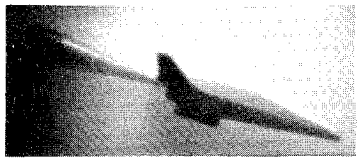

b) Electron beam photograph

Fig. 9 Ramjet fighter at 0° roll, −15° pitch.

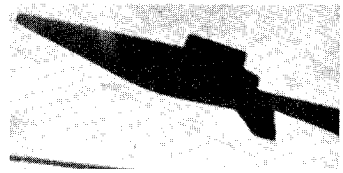

a) Schlieren photograph

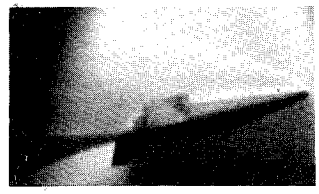

b) Electron beam photograph

Fig. 10 Ramjet fighter at 180° roll, 15° pitch.

Table I Summary of film data for schlieren and electron beam photographs

Fig.	Film type	ASA	Speed	f/no.	P_0 (psia)	Remarks
7	Polaroid 52	400	1/2 sec	6.3	300	Air blowing
8	Ektachrome 35 mm	320	16 FPS	2.3	300	Air blowing movies
9a	GAF 35 mm	500	1/500 sec	19	600	Schlieren
10a	GAF 35 mm	500	1/500 sec	19	600	Schlieren
11a	GAF 35 mm	500	1/500 sec	19	600	Schlieren
9b	Kodak Double-X 35 mm	250	24 FPS	2.2	600	Electron beam movies
10b	Kodak Double-X 35 mm	250	24 FPS	2.2	600	Electron beam movies
11b	Kodak Double-X 35 mm	250	24 FPS	2.2	600	Electron beam movies

Lifting Body

An extensive series of photographs was taken of the flowfield about the ramjet fighter aircraft configuration. The pitch-roll mechanism was set at a fixed angle of attack and the model was rolled at a constant speed of 1 rpm. Two 35 mm cameras were employed for the schlieren and electron beam photographs. The camera used for the electron beam photographs viewed the model from the side of the test cabin opposite the schlieren camera and was positioned at an angle of 60° from the horizontal; and schlieren system was placed in the horizontal plane. Reproduction of comparative frames from the schlieren and electron beam movies are shown in Figs. 9–11.

Figures 9–11 were obtained at the 600 psia operating condition. Figures 9 and 10 illustrate the "sectional view" capability of electron beam visualization. While the schlieren integrates all effects along its field of view, selective sectional regions in the plane of sweep can be examined with the electron beam.

The relative sensitivities of the schlieren and electron beam systems are well illustrated by Fig. 11. In this case, with the model rolled such that the upper surface is observed, the integration effects of the schlieren system are minimized. The shock structure does not appear in the schlieren photograph but is clearly visible with the electron beam system.

a) Schlieren photograph

b) Electron beam photograph

Fig. 11 Ramjet fighter at 270° roll, 15° pitch.

Conclusion

A sweeping electron beam fluorescence technique has been successfully applied for the first time to the visualization of hypersonic airflows. The high beam currents delivered by the duoplasmatron-electron beam generator are required for utilization of conventional photographic techniques. With this system, time resolved visualization data (i.e., high speed movies) can be obtained to allow the examination of transient flow phenomena. The ability to examine an arbitrary plane within the flowfield coupled with the capability of obtaining quantitative density measurements makes the electron beam much more versatile than conventional optical techniques for the study of complex aerodynamic configuration. In fact, high quality visualization can be obtained at density levels where double pass schlieren techniques fail to yield even the bow shock location.

Care must be used in applying the fluorescence technique to obtaining quantitative density values with photographic methods. Spectral isolation of the radiation probably will be required to obtain accurate data. The specific vibrational-rotation band employed in this case will be a function of gas density level. At low densities, a band from the N_2^+ first negative system should be used, while at high densities, a band from the N_2 second positive system must be employed.

The main disadvantage of the electron beam method is that only half of the model flowfield can be viewed at any one time. Hence, two photographs and a combined pitch and roll of the model are required to show both the compression and expansion sides of the model. This could be eliminated with a dual electron beam system but such complexity is warranted only in very special applications.

Besides being an improvement over conventional optical techniques in the low density range, the fact that the entire excited flowfield may be easily observed with the naked eye is quite convenient. Further, flowfields can be examined directly and photographed from any angle. Control of the sweeping direction allows the fluorescence technique to examine arbitrary cross-sectional slices of the flowfield.

References

[1]Rothe, D. E., "Flow Visualization Using a Traversing Electron Beam," *AIAA Journal*, Vol. 3, No. 10, Oct. 1965, pp. 1945–1946.

[2]Sebacher, D. I., "Primary and Afterglow Emission from Low Temperature Gaseous Nitrogen Exicted by Fast Electrons," *Journal of Chemical Physics*, Vol. 44, No. 11, June 1966, pp. 4131–4136.

[3]Sebacher, D. I., "Flow Visualization Using an Electron Beam Afterglow in N_2 and Air," *AIAA Journal*, Vol. 4, No. 10, Oct. 1966, pp. 1858–1859.

[4]Weinstein, L. M., Wagner, R. D., and Ocheltree, S. L., "Electron Beam Flow Visualization in Hypersonic Helium Flow," *AIAA Journal*, Vol. 6, No. 8, Aug. 1968, pp. 1623–1625.

[5]Weinstein, L. M., Wagner, R. D., Henderson, A., and Ocheltree, S. L., "Electron Beam Flow Visualization in Hypersonic Helium Flow," *International Congress on Instrumentation in Aerospace Simulation Facilities, ICIASF '69 Record*, May 1969, pp. 72–77.

[6]Muntz, E. P., "The Electron Beam Fluorescence Technique," AGARDograph 132, Dec. 1968, Neuilly-Sur-Seine, France.

[7]Maguire, B. L., Muntz, E. P., and Mallin, J. R., "Visualization Technique for Low Density Flow Fields," *IEEE Transactions on Aerospace and Electronic Systems*, Vol. AES-3, No. 2, March 1967, pp. 321–326.

[8]Petrie, S. L., Boiarski, A. A., and Lazdinis, S. S., "Electron Beam Studies of the Properties of Molecular and Atomic Oxygen," AFFDL-TR-71-30, April 1971, Air Force Flight Dynamics Lab., Wright-Patterson Air Force Base, Ohio.

[9]Rothe, D. E. and McCaa, D. J., "Emission Spectra of Molecules Gases, Excited by 10 keV Electrons," CAL 165, Dec. 1968, Cornell Aeronautical Lab., Buffalo, N.Y.